Scaling laws for localised states in a nonlocal amplitude equation

J.H.P. Dawes and C.J. Penington[1]
Department of Mathematical Sciences, University of Bath,
Claverton Down, Bath BA2 7AY, UK

December 16, 2011

Abstract

It is well known that, although a uniform magnetic field inhibits the onset of small amplitude thermal convection in a layer of fluid heated from below, isolated convection cells may persist if the fluid motion within them is sufficiently vigorous to expel magnetic flux. Such fully nonlinear ('convecton') solutions for magnetoconvection have been investigated by several authors. Here we explore a model amplitude equation describing this separation of a fluid layer into a vigorously convecting part and a magnetically-dominated part at rest. Our analysis elucidates the origin of the scaling laws observed numerically to form the boundaries in parameter space of the region of existence of these localised states, and importantly, for the lowest thermal forcing required to sustain them.

1 Introduction

Pattern formation is the often-used term for the study of the spontaneous formation of spatial structure, usually in externally driven, internally dissipative systems. Viscous fluid mechanics naturally provides many examples, not least the Rayleigh–Bénard problem of the onset and dynamics of thermal convection in a fluid layer confined in a planar layer. Such a situation has clear astrophysical and geophysical relevance as well as having become an archetypal fluid mechanical problem in its own right.

The effects of an imposed vertical magnetic field on the dynamics of convection in an electrically-conducting fluid have been explored for decades; foundational work in the area is contained and reviewed in the book by Chandrasekhar [3] and the review article by Proctor and Weiss [16]; while the former considers only the linear problem of the critical Rayleigh number for small amplitude motion, Proctor and Weiss [16] studied the nonlinear dynamics, and presented a combination of results on both the weakly nonlinear dynamics and what may be expected at finite amplitude. For an overview of work on magnetoconvection since [16] we refer the reader to the article by Weiss in this issue, and the references therein. One feature of strongly nonlinear convection discussed even in these formative times (for example by Weiss [18], Busse [2] and Proctor [14]) through numerical simulation and boundary-layer arguments, is the ability of vigorous thermally convective eddies to expel magnetic flux from their interior, sweeping it to the gaps between cells, or to the boundaries of the domain. Such dynamics, separating the domain into regions of strong magnetic field and regions of strong convection, aids our understanding of physical processes such as the formation of umbral dots within sunspots in the solar photosphere [1]. Localised states similar to umbral dots have recently been identified in numerical simulations of fully compressible 3D magnetoconvection [9], and followed using numerical continuation techniques in incompressible 2D magnetoconvection [10]. The existence of localised states in models for a variety of physical situations is discussed by Dawes [7].

In previous work on the magnetoconvection problem, Dawes [6] proposed a spatially one-dimensional 'toy model' that describes the formation of localised states in thermal convection in the presence of a magnetic field. The toy model comprises a Swift–Hohenberg equation for the vertical velocity $w(x,t)$ of the fluid at the midplane of the layer, coupled to a nonlinear diffusion equation describing the large-scale magnetic field $B(x,t)$:

$$w_t = [r - (1+\partial_x^2)^2]w - w^3 - QB^2 w, \tag{1}$$

$$B_t = \varepsilon B_{xx} + \frac{c}{\varepsilon}(Bw^2)_{xx}. \tag{2}$$

These equations are posed on the finite domain $-L/2 \le x \le L/2$, together with the assumption of periodic boundary conditions on w and B. Since the second equation takes the form of a conservation law, it is

[1]Present address: Department of Mathematics and Statistics, The University of Melbourne, Parkville, Victoria 3010, Australia

convenient to impose the constraint that the spatial average of $B(x,t)$ is (without loss of generality) unity. The trivial state $w=0$, $B=1$ undergoes a linear instability when the 'reduced Rayleigh number' $r \propto (R-R_c)/R_c$ exceeds the 'Chandrasekhar number' Q. c and ε are parameters that describe, in some sense, the strength of the nonlinear coupling of the flow to the magnetic field, and the magnetic diffusivity, respectively.

Localised states in (1) - (2) exist only if ε is sufficiently small. These states correspond to one or more vigorous convection cells that are surrounded by strong vertical magnetic field that confines them, and inhibits the onset of convective motion in the remainder of the fluid layer. The resulting bifurcation diagram that connects these fully nonlinear states together exhibits so-called 'slanted snaking' in which a localised state grows to include additional convection cells as the system evolves through a series of twists and turns and the thermal forcing is increased and decreased at successive saddle-node bifurcations.

In this paper the focus of our attention is the modulation equation

$$0 \quad = \quad \mu A + 4A_{XX} - \frac{3}{4}A^3 - \frac{qP^2A}{(1+cA^2)^{3/2}}, \tag{3}$$

which was derived in [6] through a multiple-scales analysis of (1) - (2) in the limit $\varepsilon \ll 1$. For details of the derivation we refer the reader to [6]; a very brief summary of the derivation is as follows: the analysis considers only steady-states of (1) - (2) and first integrates (2) so that the term $-QB^2w$ can be replaced by a nonlinear integral term. The multiple-scales analysis proposes a leading-order solution $w(x) = \varepsilon A(X)\sin x$, where we introduce the long length scale $X = \varepsilon x$, and proceeds to derive (3) from the solvability condition at $O(\varepsilon^3)$ in the usual way. The parameters μ and q are rescaled versions of r and Q respectively: $r = \varepsilon^2\mu$ and $Q = \varepsilon^2 q$. We point out in passing that a minor error in that paper led to the omission of the factor of $\frac{1}{4}$ in the coefficient of the A^3 term in (3). This factor can be removed by a simple rescaling of $A(X)$ and the coefficient c and has no further consequences. We note that modulational equations in similar situations were derived and explored by Matthews & Cox [12] and Proctor [15].

Equation (3) depends on four parameters: the linear driving parameter μ that physically corresponds to the rescaled reduced Rayleigh number for the thermal convection, the strength q of the magnetic field (corresponding to the Chandrasekhar number), the $O(1)$ coefficient c indicating the strength of the nonlinear flux expulsion effect compared to the diffusivity of the magnetic field, given the distinguished limit indicated by the placement of the factors of ε in (2), and the domain size L. Physical considerations imply that q, c (and L!) are positive. The coefficient P is not an independent parameter, but a functional of the amplitude $A(X)$, being defined via an integral over the finite domain $-L/2 \le X \le L/2$:

$$\frac{1}{P} \quad = \quad \frac{1}{L}\int_{-L/2}^{L/2} \frac{1}{\sqrt{1+cA^2}}\, dX. \tag{4}$$

We note in passing that the parameter c can be removed by the substitutions

$$A = \hat{A}/\sqrt{c}, \qquad X = \sqrt{c}\hat{X}, \qquad \mu = \hat{\mu}/c, \qquad q = \hat{q}/c, \qquad L = \sqrt{c}\hat{L}, \tag{5}$$

and then dropping the hats. It is easier, particularly for comparison with previous results, not to carry out this rescaling here.

Previous numerical work shows that localised states in (3) exist above a saddle-node bifurcation at critical minimum value of μ_{sn_1} that scales asymptotically approximately as $\mu_{sn_1} \sim 3.31 q^{0.503}$, i.e. with an exponent close to 1/2, in the limit of large q. Figure 1(a) shows a typical bifurcation diagram obtained for (3) using the continuation software package AUTO [8], varying μ at fixed q and c. Figure 1(b) shows the continuation of these bifurcation points in the 2-parameter plane (μ, q). The curve sn_1 is of particular interest since it corresponds to the lowest value of μ at which (for fixed q) localised states can exist. Localised states, within this amplitude equation formalism, exist between curves sn_1 and sn_3. Figure 2 shows the profiles of solutions to (3) - (4) at the points labelled a - d in figure 1(a). We note that these localised solutions lie well below the linear stability boundary $\mu = q$ at which small amplitude states bifurcate from the trivial solution.

As the domain size L increases, keeping all other parameters constant, sn_1 moves towards $\mu = 0$ and the bifurcation curve around the saddle-node bifurcation becomes sharper. In a larger domain it is easier to sustain a localised state since the expelled magnetic field increases the field strength in the remainder of the layer by a relatively smaller amount. Hence the part of the bifurcation curve between $\mu = q$ and sn_1 lies at lower and lower amplitude before increasing rapidly at sn_1 and resembling figure 2(c) over a longer section of the 'Maxwell curve' up to sn_3, as discussed in [6]; see also [10].

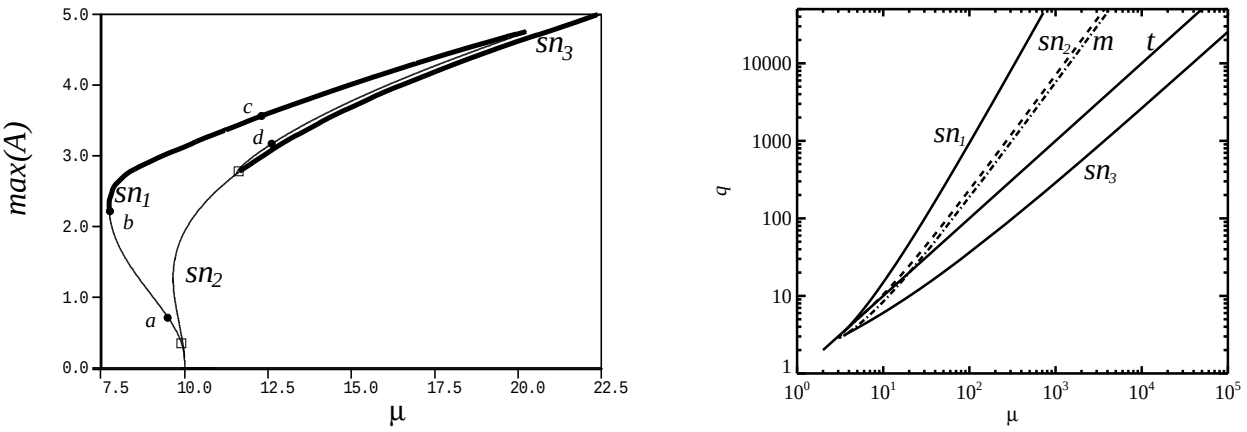

(a) (b)

Figure 1: (a) Typical bifurcation diagram for (3) - (4), plotting maximum amplitude of $A(X)$ as a function of μ for $q = 10$, $c = 0.25$, $L = 10\pi$. Labels a - d refer to the solution profiles given in the relevant part of figure 2. Thick and thin lines refer to stable and unstable solutions, respectively. (b) Bifurcation curves in the (μ, q) plane for parameter values $c = 0.25$ and $L = 10\pi$. sn_1 and sn_3 respectively denote saddle-node bifurcations on the branch of localised states. sn_2 denotes the saddle-node bifurcation on the constant amplitude branch. m denotes the location of the modulational instability at small amplitude at which the branch of localised states bifurcates from the constant solution. t denotes the linear instability at $\mu = q$.

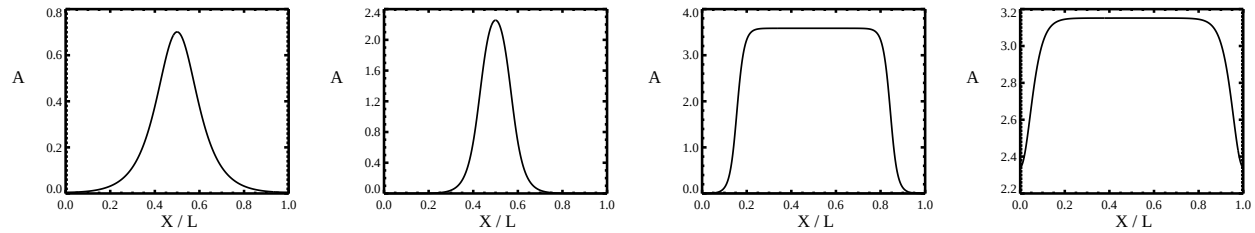

(a) (b) (c) (d)

Figure 2: Solution profiles $A(X)$ at the points labelled a - d in figure 1. Parameters: $c = 0.25$, $L = 10\pi$.

Clearly the solutions of (3) at the saddle-node bifurcation are fully nonlinear and therefore not available analytically. To make progress we investigate the asymptotic forms of (3) at large q. Numerical solutions indicate that stable equilibrium states for $A(X)$ exist in which $A(X)$ becomes very large in a part of the domain that rapidly decreases in width with increasing q; $A(X)$ decays exponentially to zero outside this thin region. Such a solution for the envelope $A(X)$ indicates both that localised states persist to arbitrarily large q and that the asymptotic form of the envelope is determined by a subtle combination of nonlinear and nonlocal constraints.

Figure 3 shows a collection of profiles of localised states as we increase q along the saddle-node curve sn_1 in figure 1(b). The solutions become progressively thinner and taller, indicating that there may be a self-similar structure to the curves. In fact, as figure 4 shows, two scalings (at least) appear relevant. Figure 4(a) indicates that the central parts of the curves collapse quite well when we plot $q^{-1/4}A$ against $q^{1/4}X$. However, figure 4(b) indicates that the tails of the localised states line up under a different scaling: plotting A against $q^{1/2}X$.

In this paper we construct approximate fully nonlinear solutions of (3) - (4) that demonstrate the interplay between these nonlinear and nonlocal effects and explain the features of the solution profiles and the curve sn_1 discussed above.

Throughout the paper we consider only time-independent solutions of (3): there are no other possible long-

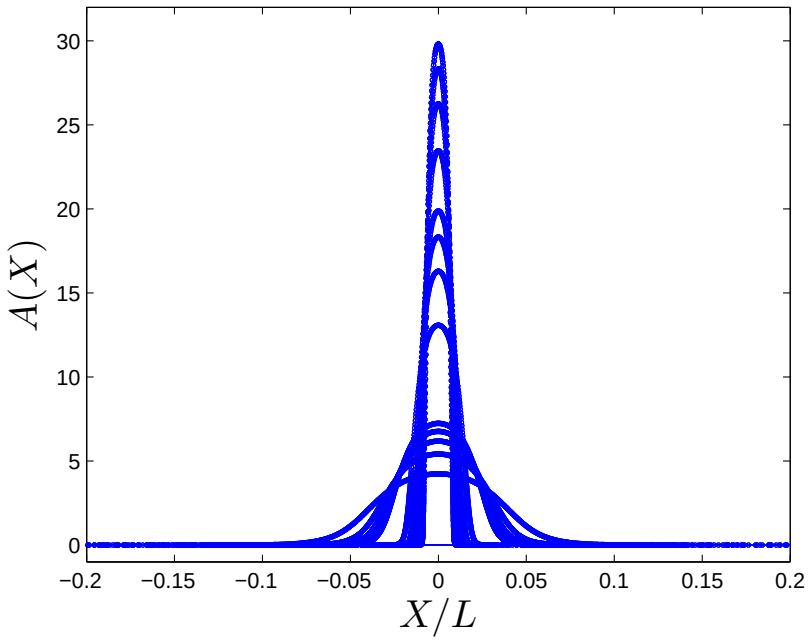

Figure 3: Profiles of equilibrium solutions $A(X)$ to (3) - (4) along the saddle-node curve sn_1 shown in figure 1(b). As q increases the solutions become increasingly tall and thin. Parameter values are $c = 0.25$ and $L = 10\pi$.

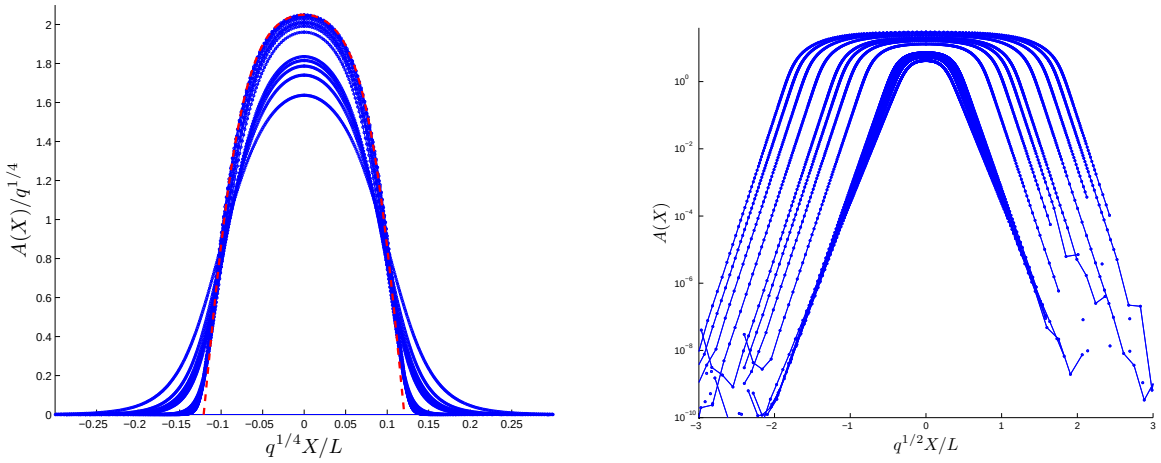

(a) (b)

Figure 4: Suggestive rescalings of the profiles in figure 3 showing appropriate scalings in the limit of large q for (a) the central large-amplitude part of the solution profile, and (b) for the small-amplitude tails. The dashed (red) curve in (a) is a snoidal curve indicating a suggestive agreement with the rescaled numerical data. Parameters: $c = 0.25$, $L = 10\pi$.

time dynamical behaviours due to the variational character of (3). Indeed, the Swift–Hohenberg model (1) - (2) from which (3) is derived cannot sustain time-dependent solutions at long times as we now show. Consider

the functional

$$\mathcal{F} \;=\; \int_{-L/2}^{L/2} \frac{1}{2}(w_{xx})^2 - (w_x)^2 + \frac{1}{2}(1-r)w^2 + \frac{1}{4}w^4 + \frac{Q}{2}B^2w^2 + \frac{\varepsilon^2 Q}{2c}B^2\,dx,$$

for which

$$\frac{\delta\mathcal{F}}{\delta w} \;=\; w_{xxxx} + 2w_{xx} + (1-r)w + w^3 + QB^2w = -w_t,$$

and

$$\frac{\delta\mathcal{F}}{\delta B} \;=\; QBw^2 + \frac{\varepsilon^2 Q}{c}B,$$

which implies that

$$B_t \;=\; \frac{c}{\varepsilon Q}\frac{\partial^2}{\partial x^2}\frac{\delta\mathcal{F}}{\delta B}.$$

Then

$$\begin{aligned}\frac{d\mathcal{F}}{dt} &= -\int_{-L/2}^{L/2}(w_t)^2\,dx + \int_{-L/2}^{L/2} B_t\frac{\delta\mathcal{F}}{\delta B}\,dx \\ &= -\int_{-L/2}^{L/2}(w_t)^2\,dx - \frac{c}{\varepsilon Q}\int_{-L/2}^{L/2}\left(\frac{\partial}{\partial x}\frac{\delta\mathcal{F}}{\delta B}\right)^2 dx \le 0,\end{aligned}$$

after an integration by parts in which the boundary term vanishes through the assumption of periodic boundary conditions. We conclude that $\mathcal{F}$ is decreasing in time unless we are at a steady solution of (1) - (2) already. From this property of (1) - (2) it is no surprise that (3) also has a variational structure. A free energy functional for which solutions of (3) are extrema is

$$\mathcal{L} \;=\; \int_{-L/2}^{L/2} -\frac{\mu}{2}A^2 + 2(A_X)^2 + \frac{3}{16}A^4\,dX \;+\; \frac{qLP}{c}, \tag{6}$$

so that (3) can be written in the form $0 = \delta\mathcal{L}/\delta A$. In section 2 we consider the form of solutions in detail, beginning with a discussion of the four possible asymptotic scalings of (3), of which two are then employed in section 3 in the construction of continuously differentiable approximate solutions to the fully nonlinear localised states. By constructing these approximate, but continuous, solutions we reproduce the numerically observed bifurcation structure and determine the correct scaling for the width of the localised state scales at large q. Section 4 discusses the properties of these approximate solutions, first in terms of the dependence of the construction parameters on μ, and then, in section 4.2, in the derivation of a scaling law for sn_1.

A contrasting approach is to make use of the variational character of the problem: in sections 5.1 and 5.2 we discuss the semi-analytical technique employed by various authors recently [11, 4, 17, 13], and known as the 'variational approximation'. The variational approximation method consists of minimising $\mathcal{L}$ over a parametrised family of functional forms that hopefully describe the structure of the localised state. It is an uncontrolled approximation in the sense that it is usually extremely difficult to propose a candidate family of solutions that can be guaranteed in a rigorous sense to approach to within a given distance of the true minimisers while retaining analytic tractability. The discussion in section 5.1 proposes a very simple piecewise-constant (discontinuous) ansatz and shows that in fact it contains enough information to yield straightforward leading-order estimates of the asymptotic scalings for the region of existence of localised states, i.e. the forms of the saddle-node bifurcation curves sn_1 and sn_3. The discussion uses (6) rather than the differential equation (3) and it circumvents the need to consider in full detail the spatial structure of solutions. A drawback of this choice of a family of piecewise-constant functions is that we are not able to establish a scaling for the width of the localised state. In section 5.2 we propose a more complicated ansatz for localised states for which we are also able, happily, to compute $\mathcal{L}$ explicitly. Even with this information, however, the scalings that apply in the limit of large q are not at all clear. However, using knowledge of the scalings that emerged in sections 2 and 3 we can identify the leading-order terms that contribute to $\mathcal{L}$: we do this in order to indicate the deficiencies in the piecewise-linear approach in section 5.1 but, even using just the leading-order terms, the completion of the calculation analytically in this case does not appear to be straightforward. A discussion of these different approaches and results is presented in section 6.

2 Asymptotic regimes

In this section we show that (3) has exactly four distinct asymptotic regimes in the limit of large q, keeping c and the domain size L fixed. These are distinguished by the asymptotic size of $A(X)$ and correspond to the centre of the large-amplitude localised state, a 'transition layer' at the outer edge of the localised state, and two intermediate regimes.

Consider the general rescaling $A(X) = q^\alpha B(\xi)$, where $\xi = q^\beta X$. Substituting gives

$$0 \quad = \quad \mu q^\alpha B + 4q^{\alpha+2\beta} B_{\xi\xi} - \frac{3}{4} q^{3\alpha} B^3 - \frac{q^{1+\alpha} P^2 B}{(1 + cq^{2\alpha} B^2)^{3/2}},$$

where clearly μ can also be rescaled to bring this term into balance with others as appropriate. We assume that P remains $O(1)$ in this analysis: we expect that this will be the case for the kinds of solution considered here in which there is always an $O(1)$ section of the domain within which $A(X)$ is not asymptotically large, and this expectation does indeed hold near sn_1. The four regimes are as follows.

Case 1. If $\alpha < 0$ then the leading order balance is $4q^{2\beta} B_{\xi\xi} \sim qP^2 B$ which implies $\beta = 1/2$.

Case 2. If $\alpha = 0$ then we find, similarly, that $\beta = 1/2$ and then $4B_{\xi\xi} \sim P^2 B/(1 + cB^2)^{3/2}$.

Case 3. If $\alpha > 0$ then it is possible to bring the B^3 term into balance with the $B_{\xi\xi}$ and nonlocal terms. This occurs for $\alpha = \beta = 1/5$ giving at leading order $4B_{\xi\xi} \sim \frac{3}{4} B^3 + P^2/(c^{3/2} B^2)$.

Case 4. For any $\alpha > 1/5$ we see that the nonlocal term is asymptotically smaller than the B^3 term: the leading order balance is given by $\alpha = \beta > 1/5$ and so $4B_{\xi\xi} \sim \frac{3}{4} B^3$.

It is clearly crucial to examine Case 4 since numerical results indicate that solutions at large q become large amplitude. Cases 2 and 3 lead to substantial difficulties in writing down appropriate solutions for the leading order form of $B(\xi)$. Case 1 is straightforward since it involves only the linearised form of (3). We therefore examine cases 1 and 4 in detail: in turns out afterwards that omission of the intermediate asymptotic regions indicated by cases 2 and 3 does not affect the scaling for the location of the saddle-node bifurcation that we deduce.

3 Construction of approximate solutions

In this section we discuss the construction of an approximate solution for $A(X)$ by patching together small and large amplitude solutions. We set $X = 0$ at the centre of the localised state and consider only even-symmetric solutions in the domain $-L/2 < X < L/2$. Symmetry and periodicity of the solution implies that we require $A_X = 0$ at both $X = 0$ and $X = \pm L/2$. The large amplitude solution occupies the 'inner' region $-X^* < X < X^*$ and the small amplitude solution occupies the 'outer' region $X^* < X < L/2$ and its symmetric counterpart.

For the outer region (case 1), the linearisation of (3) is given by

$$0 \quad = \quad \mu A + 4A_{XX} - qP^2 A, \tag{7}$$

which we use to describe the decay of $A(X)$ in the region $X^* < X < L/2$. With the Neumann boundary condition given above, (7) has the solution $A_{out}(X) = \tilde{A}_1 \cosh(\sqrt{qP^2 - \mu}(X - L/2)/2)$ for $X^* \leq X \leq L/2$ where $\tilde{A}_1$ is an undetermined constant. Given our assumption that the patch point $X = X^* \ll L/2$, A_{out} can be simplified by dropping the part that is exponentially growing in X, to give

$$A_{out}(X) = \frac{A_1}{2} \exp(-\sqrt{qP^2 - \mu} X/2). \tag{8}$$

where A_1 is a (conveniently rescaled) constant related to $\tilde{A}_1$.

Turning now to the inner region $0 \leq X \leq X^*$ in which the solution for $A(X)$ is large, we refer to case 4 above. At leading order we have the nonlinear ODE

$$0 \quad = \quad \lambda B + 4B_{\xi\xi} - \frac{3}{4}B^3,$$

where $\lambda = q^{-2\alpha}\mu$, rescaled to bring this term into balance with the $B_{\xi\xi}$ and cubic terms, $\xi = q^{\alpha}X$ and $B(\xi) = q^{-\alpha}A(X)$. We impose the symmetry boundary condition $B_{\xi} = 0$ at $\xi = 0$ which leaves the one-parameter family of solutions $B(\xi) = B_0\,\mathrm{sn}(\eta|m)$ where B_0 is the value of $B(\xi)$ at $\xi = 0$ and $\mathrm{sn}(\eta|m)$ denotes the snoidal function with argument η and parameter m. These variables are explicitly given by

$$\eta = \xi(\lambda/4 - 3B_0^2/32)^{1/2} + K(m), \qquad m = \frac{3B_0^2/32}{\lambda/4 - 3B_0^2/32}. \tag{9}$$

The shift of the origin by the constant $K(m)$ places a maximum of sn at $\xi = 0$; $K(m)$ is one quarter period of the snoidal function which we define in the usual way by the definite integral

$$K(m) = \int_0^{\pi/2} \frac{d\theta}{(1 - m\sin^2\theta)^{1/2}}.$$

Unravelling the rescalings we obtain the leading order solution in the large amplitude 'inner' regime in the form

$$A_{in}(X) \quad = \quad A_0\,\mathrm{sn}\left(\left(\frac{\mu}{4} - \frac{3A_0^2}{32}\right)^{1/2} X + K(m)\middle| m\right), \tag{10}$$

for $0 \leq X \leq X^*$, where $A(0) = A_0$ is a second undetermined constant. Note that the parameter m and the quarter period $K(m)$ remain $O(1)$ throughout this procedure, and that this is compatible with the other expressions; for example in (9), η is a sum of two $O(1)$ quantities.

We now patch together A_{in} and A_{out} at $X = X^*$: i.e. we equate the function values and their derivatives at a fixed value of the amplitude. This procedure yields a set of four algebraic equations to be solved for the four unknowns A_0, A_1, X^* and P:

$$a \quad = \quad A_{in}(X^*), \tag{11}$$

$$a \quad = \quad A_{out}(X^*), \tag{12}$$

$$A'_{in}(X^*) \quad = \quad A'_{out}(X^*), \tag{13}$$

$$\frac{1}{P} \quad = \quad \frac{2}{L}\left(\int_0^{X^*} \frac{1}{\sqrt{1 + cA_{in}(X)^2}}\,dX + \int_{X^*}^{L/2} \frac{1}{\sqrt{1 + cA_{out}(X)^2}}\,dX\right), \tag{14}$$

where we fix the constant $a = 0.1$; we have checked numerically, and we discuss further below, that the qualitative behaviour of the patched solution is not sensitive to the precise value of a used. Although these are algebraic equations, (14) involves the computation of two definite integrals. The second of these can be done analytically but the first appears to be possible only numerically. This prevents a fully analytic approach to the problem. We note that the inner and outer solutions do not, in their construction, promote any specific scaling relationship between μ and q: this is left to emerge from the algebraic system (11) - (14).

4 Results

In this section we discuss two aspects of solutions to the patching equations (11) - (14). In the first subsection we discuss details of the form of the solutions we find. In the second subsection we use (11)- (14) in the limit of large q to derive the numerically-observed scaling law $\mu \sim q^{1/2}$ for curve sn_1 as shown in figure 1(b).

4.1 Existence of localised states

Numerical results show that the patch equations (11) - (14) have two solutions, qualitatively resembling the low amplitude and large amplitude localised states, over a range of μ at sufficiently large fixed q. These localised states meet in a saddle-node bifurcation as we would anticipate.

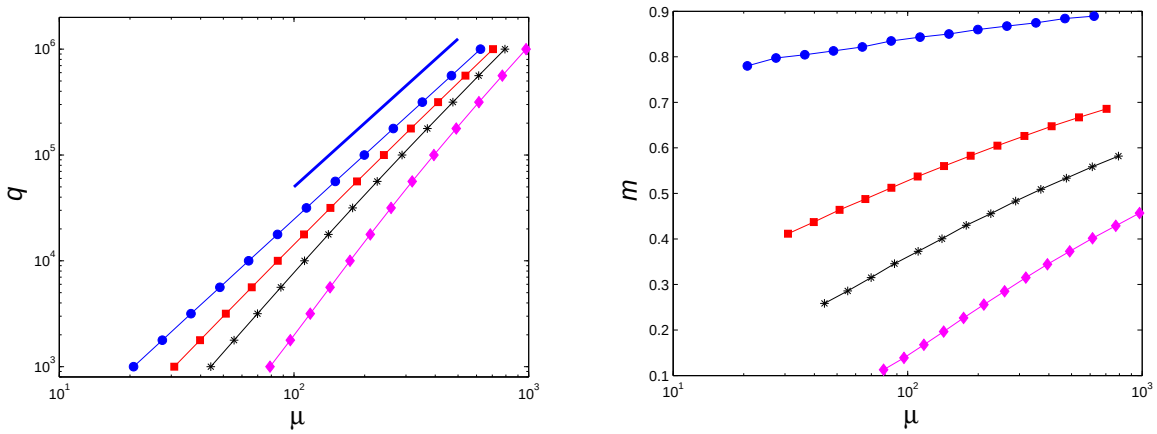

(a) (b)

Figure 5: Results of the patching approach (11) - (14) in different size domains. (a) Location of saddle-node bifurcations $\mu = \mu_{sn_1}(q)$ in the (μ, q) plane. Two localised states exist in $\mu > \mu_{sn_1}$. Short solid (blue) line has slope 2 for reference. (b) Numerically-determined values of the parameter m in patched solutions at $\mu = \mu_{sn_1}$. Results are shown for domain sizes $L = 10\pi$ (blue, dots), $L = \pi$ (red, squares), $L = \pi/2$ (black, asterisks) and $L = \pi/4$ (mauve, diamonds) are shown.

Figure 5(a) shows the location of the saddle-node bifurcation $\mu_{sn_1}(q)$ for four different fixed domain sizes L. It appears that the saddle-node bifurcation curve approaches the scaling law $\mu_{sn_1} \sim q^{1/2}$ at large q. Figure 5(b) shows the dependence of the parameter m in the snoidal function (10) at the saddle-node point. Although one might expect that $m \to 1$ in the limit $q \to \infty$, in smaller domains it appears that m approaches this limit very slowly and is neither close to unity nor close to zero, and so it may not be at all appropriate to work in either of these limits in order to simplify the snoidal function further. Or, indeed, m may remain bounded away from unity at a value dependent on the domain length L.

Figure 6 shows the evolution of (a) the patch point X^* and (b) $P - 1$ along the saddle-node bifurcation lines shown in figure 5(a). We observe that X^* and $P - 1$ both tend to zero as $q \to \infty$: these are in line with our expectations and the tall thin shape of the localised states, which allows the magnetic field strength in the remainder of the layer to relax back towards the uniform value $P = 1$ that it would take in the absence of any convective motion. Both graphs indicate decay rates that are not far from $O(q^{-1/4})$. Determination of the asymptotic behaviour at large q would depend on careful estimation of relative sizes of the integrals in (14) that we leave for future work. We observe that X^* decreases with decreasing L, but relatively weakly in absolute terms, whereas $P - 1$ increases strongly with L: these results are complementary to each other since the relatively slow decrease in the width of the localised state indicated by X^* with decreasing L requires the field in the 'outer' region to increase much more rapidly to preserve the nonlocal constraint, and hence conserve the total magnetic flux through the domain.

We now briefly comment on the role of the coefficient c which describes the strength of the flux expulsion effect (within the distinguished limit in which it is taken to be strong enough, even when produced by weakly nonlinear convection, to balance the linear diffusion of magnetic field) which appears in the patching conditions (11) - (14) only in the integral expressions for P in (14). In moderate or large domains, at large q the first term will make only a small contribution to the right hand side, since $A(X)$ becomes large within $O \leq X \leq X^*$ and X^* itself tends to zero. So the right hand side is dominated by the second integral which has an $O(1)$ value since $A(X)$ is decaying in the outer region. Hence the overall influence of c on the value of P, and thereby on the solution, appears to be almost negligible unless the domain is comparable with the size of the localised state. We will see in later sections that sn_1 has in fact a non-trivial dependence on c which is not revealed by the above argument. In the present context the dependence of the location of sn_1 on c is obscured by the free parameter a that cannot be independently determined: a contains implicitly a dependence on c that this approach does not identify.

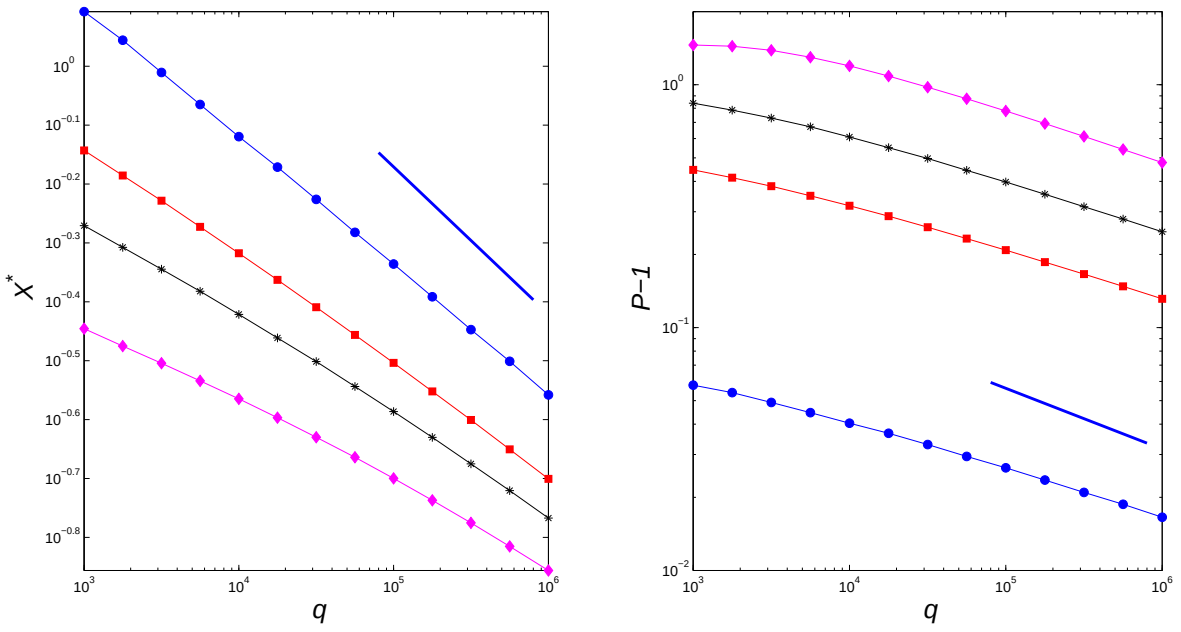

(a) (b)

Figure 6: Evolution of (a) X^* and (b) $P-1$ at the saddle-node point $\mu = \mu_{sn}(q)$, with increasing q and for different size domains. Results are shown for domain sizes $L = 10\pi$ (blue, dots), $L = \pi$ (red, squares), $L = \pi/2$ (black, asterisks) and $L = \pi/4$ (mauve, diamonds) are shown. Short (blue) lines have slope -0.25 in both cases.

4.2 Derivation of the scaling law for μ_{sn_1}

Finally, the patching approach enables us to explain the origin of the scaling law $\mu_{sn_1} \sim q^{1/2}$ as follows. First, note that since a is fixed and the amplitude A_0 at the saddle-node point is increasing (since μ is increasing), the snoidal function must be becoming small, and hence its argument must be approaching $2K$. Therefore we examine the behaviour of $\mathrm{sn}(y|m)$ near its zeros. We recall the Taylor series expansion for $\mathrm{sn}(y|m)$ about $y = 0$:

$$\mathrm{sn}(y|m) \quad = \quad y - (1+m)\frac{y^3}{3!} + \cdots$$

and the symmetry properties of $\mathrm{sn}(y|m)$:

$$\mathrm{sn}(2K + y|m) = \mathrm{sn}(-y|m) = -\mathrm{sn}(y|m).$$

Note next that the patching conditions (11) - (13) can be combined to give the alternative constraint

$$\frac{A'_{in}(X^*)}{A_{in}(X^*)} \quad = \quad \frac{A'_{out}(X^*)}{A_{out}(X^*)},$$

which, using the Taylor expansions given above can be written explicitly, at leading order, as

$$\frac{-(\mu/4 - 3A_0^2/32)^{1/2}}{K - (\mu/4 - 3A_0^2/32)^{1/2}X^*} \quad = \quad -q^{1/2}\frac{P}{2}. \tag{15}$$

Now let $\mu = \lambda q^{2\alpha}$ where we suppose that $\alpha > 0$. Numerical results (for example figure 5b) indicate that, at least in sufficiently large domains, m approaches unity as $q \to \infty$; hence from (9) we estimate that $A_0^2 \sim 4\lambda q^{2\alpha}/3$. We combine (15) with the first patching condition (11) and simplify as follows:

$$a = A_{in}(X^*) = A_0 \,\mathrm{sn}\left(\left(\frac{\mu}{4} - \frac{3A_0^2}{32} \right)^{1/2} X^* + K \middle| m \right),$$

and so, using (15) and symmetry properties of sn we have

$$a = A_0 \,\mathrm{sn}\left(2K - \frac{2}{Pq^{1/2}}\left(\frac{\mu}{4} - \frac{3A_0^2}{32}\right)^{1/2}\middle| m\right) = A_0 \,\mathrm{sn}\left(\frac{2}{Pq^{1/2}}\left(\frac{\mu}{4} - \frac{3A_0^2}{32}\right)^{1/2}\middle| m\right),$$

Hence, asymptotically we obtain

$$a \sim \left(\frac{4\lambda}{3}\right)^{1/2} q^{\alpha} \,\mathrm{sn}\left(\frac{2}{Pq^{1/2}}\left(\frac{\lambda}{8}q^{2\alpha}\right)^{1/2}\middle| m\right).$$

In the limit of large q we observe that the first argument of $\mathrm{sn}(\cdot|\cdot)$ tends to zero if $0 < \alpha < 1/2$ in which case

$$a \sim \left(\frac{4\lambda}{3}\right)^{1/2} q^{\alpha} \frac{2}{Pq^{1/2}}\left(\frac{\lambda}{8}q^{2\alpha}\right)^{1/2}.$$

Therefore the required asymptotic scaling must be $\alpha = 1/4$: this balances the scalings so that a remains $O(1)$ as $q \to \infty$. Moreover we deduce that $a = \sqrt{2/3}\lambda$ since $P \to 1$ as $q \to \infty$. We conclude that the saddle-node bifurcation point $\mu_{sn} = \lambda q^{2\alpha}$ scales as $q^{1/2}$ at large q. We note that this conclusion is consistent with our initial assumptions above since the scaling $\mu_{sn} = O(q^{1/2})$ implies $A_0 = O(q^{1/4}) \gg q^{1/5}$ as required for the scalings of Case 4 (see section 2).

From (15) we see also that the width parameter X^* must scale as $X^* \sim q^{-1/4}$, since $K(m)$ is $O(1)$ and $K - (\mu/4 - 3A_0^2/32)^{1/2}X^* \sim q^{-1/4}$. This is also in line with Case 4. Reversing the rescaling (5), noted in section 1, that removes the parameter c we see that $X^* \sim q^{-1/4}$ implies $X^*/\sqrt{c} \sim (cq)^{-1/4}$ and hence $X^* \sim (c/q)^{1/4}$. Figure 7 confirms this asymptotic dependence on c along sn_1, at fixed q. The data collapse

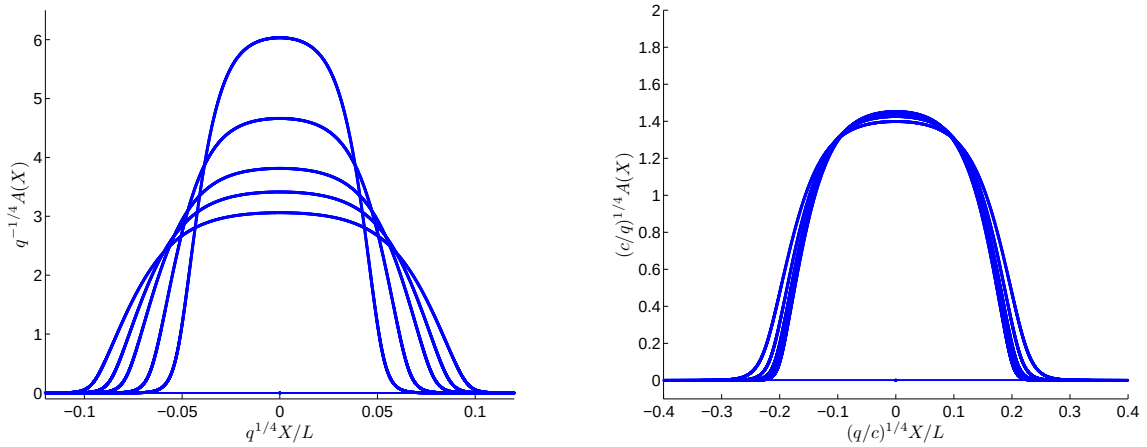

(a) (b)

Figure 7: Localised states on sn_1 obtained using AUTO for c in the range $0.003 < c < 0.05$ at $q = 100\,000$ and $L = 10\pi$. (a) Solutions $A(X)$ scaled only by q, showing systematic decrease in height and increase in width as c increases. (b) Solutions $A(X)$ rescaled by appropriate additional factors of $c^{1/4}$.

in figure 7(b) is not complete since the domain size L remains fixed as c varies instead of being rescaled in accordance with (5).

5 Variational approximations

In this section we exploit the variational nature of (3) and minimise the Langrangian $\mathcal{L}$ over families of very simple functions that describe, in broad terms, the shape of localised solutions to (3). These functional families are chosen for their analytic simplicity; they are not pointwise correct, even asymptotically as q becomes large. However, since $\mathcal{L}$ may be computed explicitly, they enable us to estimate the scaling laws associated with the

saddle-node bifurcation curves sn_1 and sn_3. This 'variational approximation' approach works by replacing the requirement that equilibrium solutions of (3) extremise the functional $\mathcal{L}$ with the requirement that, when $A(X)$ is restricted to a the finite-dimensional subspace of functional forms having a fixed number of real parameters, $\mathcal{L}$ is at stationary point with respect to those parameters. The first family that we minimise over consists of piecewise-constant functions: this is analytically extremely simple but lacks even continuity of the solutions (in X). The second family, discussed in section 5.2, is continuous (but not differentiable), and depends on an additional parameter which describes the slope of the (sharp) transition between the large-amplitude centre of the localised state and the small-amplitude tail.

5.1 Piecewise constant approximation

In this first subsection we propose the 'top-hat' ansatz for $A(X)$ that describes a localised state of length ℓ and amplitude A_0 within a domain of length L. The solution therefore contains two free parameters: A_0 and ℓ over which we minimise $\mathcal{L}$:

$$A(X) \quad = \quad \begin{cases} A_0 \ \text{ in } \ |X| < \ell/2, \\ 0 \ \text{ in } \ \ell/2 < |X| \leq L/2. \end{cases} \tag{16}$$

With this ansatz we obtain, explicitly,

$$P \quad = \quad \frac{L(1+cA_0^2)^{1/2}}{\ell + (L-\ell)(1+cA_0^2)^{1/2}},$$

and so

$$\mathcal{L} \quad = \quad -\frac{\mu}{2}A_0^2\ell + \frac{3}{16}A_0^4\ell + \frac{qL^2}{c}\frac{(1+cA_0^2)^{1/2}}{\ell + (L-\ell)(1+cA_0^2)^{1/2}}. \tag{17}$$

The requirement that $A(X)$ minimises $\mathcal{L}$ now becomes the requirement that $\mathcal{L}$ is (locally) minimised over ℓ and A_0. Computing $\partial\mathcal{L}/\partial\ell$ and $\partial\mathcal{L}/\partial A_0$ we obtain

$$\frac{\partial\mathcal{L}}{\partial\ell} \quad = \quad -\mu A_0^2 + \frac{3A_0^4}{8} - \frac{2qL^2(1+cA_0^2)^{1/2}}{c}\frac{[1-(1+cA_0^2)^{1/2}]}{[\ell+(L-\ell)(1+cA_0^2)^{1/2}]^2}, \tag{18}$$

$$\frac{\partial\mathcal{L}}{\partial A_0} \quad = \quad -\mu A_0\ell + \frac{3A_0^3\ell}{4} + \frac{2qL^2}{c}\left[\frac{cA_0(1+cA_0^2)^{-1/2}}{\ell+(L-\ell)(1+cA_0^2)^{1/2}} - \frac{cA_0(L-\ell)}{[\ell+(L-\ell)(1+cA_0^2)^{1/2}]^2}\right]. \tag{19}$$

We now investigate solutions of these equations for A_0 and ℓ in the limit of large q and μ (and, therefore, in the limit of large amplitude A_0). First, we note that the form of P in the limit of large A_0:

$$P \quad \sim \quad \frac{A_0\sqrt{c}L}{\ell + (L-\ell)A_0\sqrt{c}},$$

indicates there are two possible asymptotic limits: if $L-\ell \sim 1$ then $P \sim L/(L-\ell)$ remains $O(1)$ as $A_0 \to \infty$, or if $L-\ell = \hat{\ell}/A_0 \ll 1$ (defining $\hat{\ell}$ to be an $O(1)$ constant) then $P \sim A_0L\sqrt{c}/(\ell+\hat{\ell}\sqrt{c}) = O(A_0) \gg 1$.

In either case, requiring both (18) and (19) to be zero leads to the requirement that

$$\left(\mu A_0^2 - \frac{3A_0^4}{8}\right)c \quad = \quad \left[(1+cA_0^2)^{1/2} - 1\right]\left(\mu - \frac{3A_0^2}{4}\right)(1+cA_0^2),$$

which, at large A_0, implies that

$$\mu - \frac{3A_0^2}{8} \quad = \quad A_0c\sqrt{c}\left(\mu - \frac{3A_0^2}{4}\right), \tag{20}$$

and hence $\mu \sim 3A_0^2/4$. Now, in the first limit, in which $L-\ell \sim 1$ we substitute this into (18) and obtain

$$\mu \sim \left(\frac{3q}{c}\right)^{1/2}\frac{L}{L-\ell}. \tag{21}$$

In the second limit, in which $L-\ell=O(A_0)$, we find that (18) implies the different scaling law

$$\mu \sim 4q\frac{L^2}{(L+\hat{\ell}\sqrt{c})^2}. \tag{22}$$

At large q, therefore, we expect localised states to exist over the region between the curves (21) and (22). The limits of this region, at fixed q, are given by taking $\ell=0$ in (21) and $\hat{\ell}=0$ in (22) which yields estimates for the locations of the saddle-node curves sn_1 and sn_3: $\mu\sim\sqrt{3q/c}$ and $\mu\sim 4q$, respectively. These are in good agreement with the numerical results reported in [6] for which $c=0.25$: $\mu\sim 3.31q^{0.503}$ and $\mu\sim 3.41q^{1.01}$ respectively. A further check that is available is that the scaling laws must also be compatible with the rescaling (5): the procedure of setting c to unity and then rescaling $(\mu,q)\to(c\mu,cq)$ should leave invariant an asymptotic relation between μ and q invariant. So if we suppose a scaling law $\mu\sim q^{\delta}c^{\delta_0}$ for some exponents δ, δ_0 then for compatibility we must in fact have $\delta_0=\delta-1$, i.e. $\mu\sim q^{\delta}c^{\delta-1}$. For sn_1 we have a relation of this form with $\delta=1/2$; for sn_3 we have the case $\delta=1$.

The argument above does not, however, enable us to determine the width of the localised states near sn_1 and sn_3; for example, it is not possible to deduce an asymptotic relation between $\hat{\ell}$ and q as $\hat{\ell}\to 0$.

5.2 An improved ansatz

In this subsection we carry out a very similar calculation to that in section 5.1 but using a continuous solution ansatz. This calculation suffers from the same underlying difficulty as that in section 5.1 in that we cannot estimate the accuracy of the functional form as a true minimiser of the Lagrangian $\mathcal{L}$. However, the computation is of interest as a comparison with the results of section 5.1; one might hope that the same scaling laws at large q were indicated using this ansatz as in previous sections, and we indicate how the results link together although, due to the more complicated computations involved, we cannot provide a complete analytical solution to the variational approximation in the case studied here.

Motivated by [13] and in particular by the more straightforward case of the (local) cubic-quintic Ginzburg–Landau equation, for which it is an exact solution, at the Maxwell point, for a stationary front, we propose the continuous solution ansatz

$$A(X) \;=\; \frac{\hat{A}}{\sqrt{1+\mathrm{e}^{b(|X|-\ell/2)}}}, \tag{23}$$

in the domain $-L/2\le X\le L/2$, where $\hat{A}$, b and ℓ are again positive parameters over which we will minimise $\mathcal{L}$. Note that such a solution $A(X)$ attains values close to $\hat{A}$ near $X=0$ in a sufficiently large domain, before dropping rapidly to zero when $|X|\gg\ell/2$. Therefore the overall width of the localised state is close to ℓ. Although the ansatz is continuous, it is not differentiable at $X=0$, in the centre of the localised state; since we expect gradients here to be close to zero the discontinuity in gradient is expected to be small.

Substituting this ansatz into (6) we obtain exact results for the terms in $\mathcal{L}$ as follows:

$$\begin{aligned}
\int_{-L/2}^{L/2}-\frac{\mu}{2}A^2\,dX &= -\frac{\mu\hat{A}^2}{2b}\left[\log\left(\frac{f_L-1}{f_0-1}\right)-\log\left(\frac{f_L}{f_0}\right)\right],\\
\int_{-L/2}^{L/2}2(A_X)^2\,dX &= \frac{\hat{A}^2 b}{2}\left(\frac{1}{2f_L^2}-\frac{1}{f_L}-\frac{1}{2f_0^2}+\frac{1}{f_0}\right),\\
\int_{-L/2}^{L/2}\frac{3}{16}A^4\,dX &= \frac{3\hat{A}^4}{16b}\left[\log\left(\frac{f_L-1}{f_0-1}\right)-\log\left(\frac{f_L}{f_0}\right)+\frac{1}{f_L}-\frac{1}{f_0}\right],\\
\frac{qLP}{c} &= \frac{qL^2}{4c(F(L)-F(0))},
\end{aligned}$$

where $f_L=1+\mathrm{e}^{b(L-\ell)/2}$, $f_0=1+\mathrm{e}^{-b\ell/2}$,

$$\begin{aligned}
F(x) \;=\;& \frac{1}{b}\log\left(\frac{1}{2}c\hat{A}^2+f_x+\sqrt{f_x^2+c\hat{A}^2f_x}\right)\\
&-\frac{1}{b\sqrt{1+c\hat{A}^2}}\log\left(f_x(2+c\hat{A}^2)+c\hat{A}^2+2\sqrt{(1+c\hat{A}^2)(f_x^2+c\hat{A}^2f_x)}\right)+\frac{x-\ell}{\sqrt{1+c\hat{A}^2}},
\end{aligned}$$

and $f_x = 1 + \mathrm{e}^{b(x-\ell)}$. In principle one could proceed exactly as in section 5.1 and attempt to solve simultaneously the equations $\partial\mathcal{L}/\partial\hat{A} = \partial\mathcal{L}/\partial b = \partial\mathcal{L}/\partial\ell = 0$. It is of more interest in the present context first to attempt to identify the leading-order contributions to $\mathcal{L}$ at large q.

Such an exercise is made much more straightforward by the adoption of the scalings identified in section 2. These imply that as $q \to \infty$, near sn_1, we expect $\hat{A} \sim b \sim 1/\ell \sim q^{1/4}$ since (i) the amplitude in the centre of the localised state $A(0)$ should be close to $\hat{A}$, (ii) the second derivative term remains part of the leading-order balance in the large-amplitude region (Case 4 in section 2) and (iii) the width ℓ of the localised state tends to zero with the same scaling as X^* did in section 4. Computing the leading-order terms in $\mathcal{L}$ in this distinguished limit we obtain

$$\begin{aligned}
\mathcal{L} &\sim \left(\frac{3\hat{A}^4}{8b} - \frac{\mu\hat{A}^2}{b}\right)\left[\frac{b\ell}{2} + \log\left(1+\mathrm{e}^{-b\ell/2}\right)\right] - \frac{3\hat{A}^4}{8b}\frac{1}{1+\mathrm{e}^{-b\ell/2}} \\
&\quad + \hat{A}^2 b\left[\frac{1}{1+\mathrm{e}^{-b\ell/2}} - \frac{1}{2\left(1+\mathrm{e}^{-b\ell/2}\right)^2}\right] + \frac{qL^2}{c(L-\ell)}, \\
\mathcal{L} &\sim -\frac{\mu}{2}\hat{A}^2\ell + \frac{3}{16}\hat{A}^4\ell + \frac{qL^2}{c(L-\ell)} + \left(\frac{3\hat{A}^4}{8b} - \frac{\mu\hat{A}^2}{b}\right)\log\left(1+\mathrm{e}^{-b\ell/2}\right) - \frac{3\hat{A}^4}{8b}\frac{1}{1+\mathrm{e}^{-b\ell/2}} \\
&\quad + \hat{A}^2 b\left[\frac{1}{1+\mathrm{e}^{-b\ell/2}} - \frac{1}{2(1+\mathrm{e}^{-b\ell/2})^2}\right]. \qquad (24)
\end{aligned}$$

The first three terms in (24) closely resemble the terms in (17) resulting from the piecewise-constant approximation; they agree exactly if the limit of large A_0 is applied to the last term in (17). Note that if $\mu^{1/2} \sim \hat{A} \sim b \sim 1/\ell \sim q^{1/4}$ then $\mathrm{e}^{-b\ell/2}$ remains $O(1)$ as q becomes large, and every term in (24) is $O(q^{3/4})$ apart from $qL^2/(c(L-\ell))$ which is $O(q)$, and so terms in (24) after the first three cannot be ignored. Hence, unfortunately, we cannot deduce a simple expression for the scaling law for sn_1 directly from this expression. With the additional assumption that $b\ell$ remains sufficiently large in the limit described above, near sn_1, that we can take $\mathrm{e}^{-b\ell/2}$ to be small, we can at least show that (24) indicates at leading order the same scaling law (21) for sn_1 as in the previous section. Starting from (24 and assuming that $\mathrm{e}^{-b\ell/2}$ is small we obtain

$$\mathcal{L} \sim -\frac{\mu}{2}\hat{A}^2\ell + \frac{3}{16}\hat{A}^4\ell + \frac{qL^2}{c(L-\ell)} - \frac{\mu\hat{A}^2}{b}\mathrm{e}^{-b\ell/2} - \frac{3\hat{A}^4}{32} + \frac{3\hat{A}^4}{4b}\mathrm{e}^{-b\ell/2} + \frac{1}{2}\hat{A}^2 b + O(\mathrm{e}^{-b\ell}).$$

From this simplified expression we compute

$$\begin{aligned}
\frac{\partial\mathcal{L}}{\partial\ell} &= -\frac{\mu}{2}\hat{A}^2 + \frac{3}{16}\hat{A}^4 + \frac{qL^2}{c(L-\ell)^2} + \frac{\mu\hat{A}^2}{2}\mathrm{e}^{-b\ell/2} - \frac{3\hat{A}^4}{8}\mathrm{e}^{-b\ell/2} + O(\mathrm{e}^{-b\ell}), \\
\frac{\partial\mathcal{L}}{\partial\hat{A}} &= -\mu\hat{A}\ell + \frac{3}{4}\hat{A}^3\ell - \frac{2\mu\hat{A}}{b}\mathrm{e}^{-b\ell/2} - \frac{3\hat{A}^3}{2b} + \frac{3\hat{A}^3}{b}\mathrm{e}^{-b\ell/2} + \hat{A}b + O(\mathrm{e}^{-b\ell}).
\end{aligned}$$

Equating these with zero and eliminating $\mathrm{e}^{-b\ell/2}$ we obtain

$$\left(\frac{\mu}{2}\hat{A}^2 - \frac{3}{16}\hat{A}^4 - \frac{qL^2}{c(L-\ell)^2}\right)\left(\frac{3\hat{A}^2}{b} - \frac{2\mu}{b}\right) = \hat{A}^2\left(\frac{\mu}{2} - \frac{3\hat{A}^2}{8}\right)\left(\mu\ell - \frac{3}{4}\hat{A}^2\ell + \frac{3\hat{A}^2}{2b} - b\right).$$

In the limit $\hat{A} \sim b \gg 1$ we expect that the last two terms in the second set of parentheses on the right hand side are subdominant as long as ℓ does not become too small too quickly. Then a consistent collection of limiting behaviours is that $\mu \sim \frac{3}{4}\hat{A}^2$ - in fact there is a double root on the right hand side, and hence the terms in the first set of parentheses on the left hand side must also vanish. This implies $3\hat{A}^4/16 = qL^2/(c(L-\ell)^2)$ which in turn implies (21).

Figure 8 compares the results of the two variational approximation calculations with numerical results, computed using AUTO, for the location of the saddle-node curve sn_1. Figure 8(a) shows results for a domain of length $L = 10\pi$ while figure 8(b) compares the results for the continuous approximation (23) in the cases $L = 10\pi$ and $L = \pi$. For $L = 10\pi$ we observe that the continuous ansatz (23) produces an extremely accurate estimate of the location of sn_1, and even the piecewise-constant ansatz produces a very good guide if $q > 10^2$. In agreement with intuition and figure 5(a) we see that in smaller domains the sn_1 curve shifts to larger μ, but not by much since the width of the localised states is rapidly becoming small as q increases while L remains fixed.

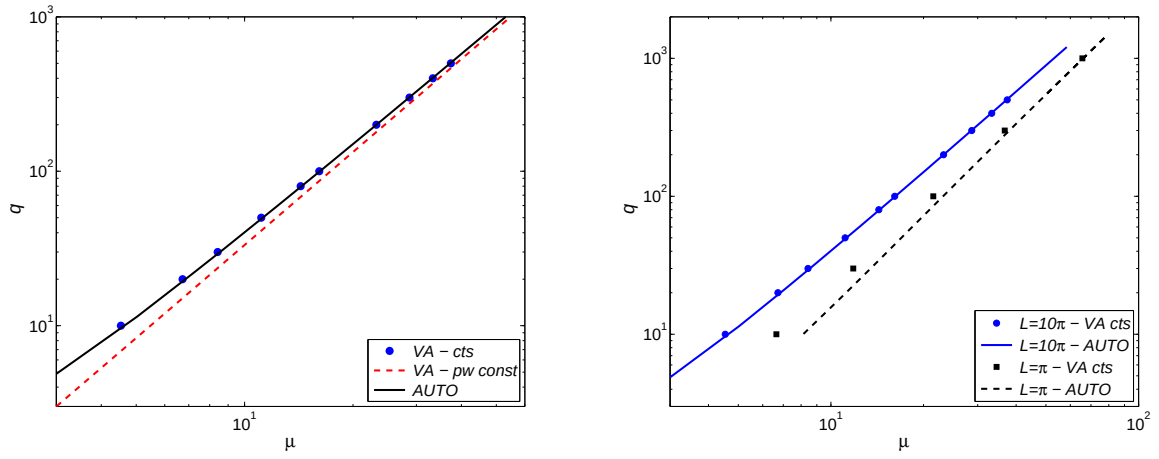

(a) (b)

Figure 8: Comparison of estimates for the location of sn_1 in the (μ, q) plane for $c = 1$. (a) $L = 10\pi$: numerical location of sn_1 computed using AUTO (solid black line); red dashed line indicates the estimate using the ansatz (16); blue circles indicate estimates using the ansatz (23). (b) $L = 10\pi$: numerical location of sn_1 computed using AUTO (solid blue line); blue dots indicate estimates using the ansatz (23). $L = \pi$: numerical location of sn_1 computed using AUTO (dashed black line); black squares indicate estimates using the ansatz (23).

6 Discussion

In this paper we have computed approximate fully nonlinear solutions to the nonlocal nonlinear envelope (modulation) equation derived in [6] for localised states in a model for magnetoconvection. These calculations explain analytically scaling laws that were observed numerically in [6]. We have shown semi-analytically, through different approximate solution methods, that the scaling law for the saddle-node bifurcation which gives the lowest value of the thermal forcing μ at which fully nonlinear localised states can persist scales as $\mu = O(q^{1/2})$ in a robust way for the model equations (3) - (4). This agrees with the observed scaling in the model extended Swift–Hohenberg equation (1) - (2) considered in [6].

While the patching method feels more reliable, in terms of considering the spatial construction of the solution $A(X)$ over the whole domain and its asymptotic behaviour, it has its obvious drawbacks: most obviously in the the omission of two of the four asymptotic regimes and the need to pick a value of $A(X)$ at which to match the values and first derivatives of the inner and outer solutions. This leads to the existence of an undetermined parameter in the numerical method. Perhaps luckily, the choice of this constant does not affect the exponent in the scaling law at which the saddle-node bifurcation takes place. The patching method contains the initial ingredients of a proper matched asymptotics approach to the problem, and it is perhaps a useful first step in that direction. It is also able, although we mentioned this only in passing, to construct the low-amplitude unstable localised states between the points labelled a and b on figure 1(a).

The variational approximation produces surprisingly good results from very simple initial proposals for the structure of localised solutions. This provides a vivid indication of the strength of the variational nature of the problem in constraining its behaviour: even the picewise constant solution ansatz considered in section 5.1 picks out exactly those details of the form of the solution that determine the bifurcation diagram (at least at large q) and ignores many details that do not contribute at leading order. Although one might expect that a method that in some sense carries out an averaging procedure will be able to extract a leading-order scaling in an efficient fashion, there is a no guarantee that an *a priori* ansatz *a là* (16) will succeed.

Comparing the two methods qualitatively, we note that the estimates from the variational approximation as shown in figure 8 have a slight positive curvature at smaller μ and tend to the asymptotic scaling $\mu \sim q^{1/4}$ from above, which is in agreement with the numerical results from AUTO. The patching results, in contrast, have a negative curvature and tend to the asymptotic result from below, as shown in figure 5(a).

An appropriate choice of the free parameter a in the patching method, enables us to match the asymptotic leading-order result for sn_1 with that given by the variational method. This leads to a necessary condition

for the patching method to work; the patching level a must be below the maximum $A_0 = A(0)$ as predicted by the variational approximation. At large q this is not expected to cause difficulty since a remains $O(1)$ as $q \to \infty$ while A_0 increases as $q^{1/4}$. To confirm the role of c in this comparison at the saddle-node point $\mu_{sn_1} = \sqrt{3q/c}$ we note that $a = \sqrt{2/3}\mu_{sn_1} q^{-1/2}$ from section 4.2, while $A_0^2 = 4/\sqrt{3cq}$ from section 5.1. So the requirement that $a < A_0$ turns out to require $cq > 3/4$. This is clearly the case for the values of c considered above.

Turning to the broader context of magnetoconvection in an incompressible viscous fluid it is not clear that the scaling $\mu_{sn_1} \propto q^{1/2}$, i.e. $r \propto \varepsilon Q^{1/2}$ where ε is the magnetic Prandtl number η/κ, actually matches that observed in numerical simulations of (truncated models for) magnetoconvection [5]. There is clearly more detailed work remaining to be carried out in order to elucidate the details of magnetoconvection which are not captured by the model problem (1) - (2) but which do affect these scaling laws for strongly nonlinear solutions.

Acknowledgements

JHPD gratefully acknowledges the support of the Royal Society through a University Research Fellowship, and thanks Douglas Gough, Mike Proctor and Nigel Weiss for useful discussions and comments. CJP was supported by the EPSRC. Both authors are grateful to the anonymous referees for their comments on an earlier version of this paper.

References

[1] S.M. Blanchflower, Magnetohydrodynamic convectons. *Phys. Lett.* A **261**, 74–81 (1999)

[2] F.H. Busse, Nonlinear interaction of magnetic field and convection. *J. Fluid Mech.* **71**, 193–206 (1975)

[3] S. Chandrasekhar, *Hydrodynamic and Hydromagnetic Stability.* Oxford University Press (1961), republished by Dover Publications, Inc. (1981)

[4] C. Chong and D.E. Pelinovsky, Variational approximations of bifurcations of asymmetric solitons in cubic–quintic nonlinear Schrödinger lattices. *Discrete and Continuous Dynamical Systems* Series S **4**, 1019–1031 (2011)

[5] J.H.P. Dawes, Localized states in thermal convection with an imposed vertical magnetic field. *J. Fluid Mech.* **570**, 385–406 (2007)

[6] J.H.P. Dawes, Localised pattern formation with a large-scale mode: slanted snaking. *SIAM J. Appl. Dyn. Syst.* **7**, 186–206 (2008)

[7] J.H.P. Dawes, The emergence of a coherent structure for coherent structures: localized states in nonlinear systems. *Phil. Trans. R. Soc.* A **368**, 3519–3534 (2010)

[8] E. J. Doedel, A. R Champneys, T. Fairgrieve, Y. Kuznetsov, B. Oldeman, R. Paffenroth, B. Sandstede, X. Wang, and C. Zhang, *AUTO-07p: Continuation and Bifurcation Software for Ordinary Differential Equations*, 2007; software available to download from `http://indy.cs.concordia.ca/auto/`.

[9] S.M. Houghton and P.J. Bushby, Localized plumes in three-dimensional compressible magnetoconvection. *Mon. Not. R. Astr. Soc.* **412** 555–560 (2011)

[10] D. Lo Jacono, A. Bergeon and E. Knobloch, Magnetohydrodynamic convectons. Preprint.

[11] B.A. Malomed, Variational methods in nonlinear fiber optics and related fields. *Prog. Opt.* **43**, 71–193 (2002)

[12] P.C. Matthews and S.M. Cox, Pattern formation with a conservation law. *Nonlinearity* **13**, 1293–1320 (2000)

[13] P.C. Matthews and H. Susanto, Variational approximations to homoclinic snaking in continuous and discrete systems. *Preprint* (2011)

[14] M.R.E. Proctor, Collective bifurcation of flux sheets in two-dimensional magnetoconvection. *Mon. Not. R. Astr. Soc.* **204** 935–943 (1983)

[15] M.R.E. Proctor, Finite amplitude behaviour of the Matthews-Cox instability. *Phys. Lett.* A **292** 181–187 (2001)

[16] M.R.E. Proctor and N.O. Weiss, Magnetoconvection. *Rep. Prog. Phys.* **45**, 1317–1379 (1982)

[17] H. Susanto and P.C. Matthews, Variational approximations to homoclinic snaking. *Phys. Rev.* E **83**, 035201(R) (2011)

[18] N.O. Weiss, The expulsion of magnetic flux by eddies. *Proc. R. Soc. Lond.* A **293**, 310–328 (1966)